

Improving RRT for Automated Parking in Real-world Scenarios

Jiri Vlasak, Michal Sojka, and Zdeněk Hanzálek

Source code: <https://rtime.ciirc.cvut.cz/gitweb/hubacji1/iamcar2.git>
Video: https://www.youtube.com/watch?v=u_Vqfd5Cn8Q

Improving RRT for Automated Parking in Real-world Scenarios

Jiri Vlasak^{12*}, Michal Sojka^{2†}, and Zdeněk Hanzálek^{2‡}

¹Faculty of Electrical Engineering, Czech Technical University in Prague

²Czech Institute of Informatics, Robotics and Cybernetics, Czech Technical University in Prague

{jiri.vlasak.2, michal.sojka, zdenek.hanzalek}@cvut.cz

Abstract

Automated parking is a self-driving feature that has been in cars for several years. Parking assistants in currently sold cars fail to park in more complex real-world scenarios and require the driver to move the car to an expected starting position before the assistant is activated. We overcome these limitations by proposing a planning algorithm consisting of two stages: (1) a geometric planner for maneuvering inside the parking slot and (2) a Rapidly-exploring Random Trees (RRT)-based planner that finds a collision-free path from the initial position to the slot entry. Evaluation of computational experiments demonstrates that improvements over commonly used RRT extensions reduce the parking path cost by 21% and reduce the computation time by 79.5%. The suitability of the algorithm for real-world parking scenarios was verified in physical experiments with Porsche Cayenne.

Keywords: Automated vehicle, real-world parking, Rapidly-Exploring Random Trees

1 Introduction

The automotive industry is currently experiencing the boom of self-driving cars. We still have to wait for fully automated cars, but the level of automation is increasing every year and advanced features such

as adaptive cruise control, lane departure warning or parking assistance are available in more and more car models.

The parking assistants currently available in production vehicles suffer from several limitations. They force the driver to stop the car in a certain position with respect to a parking slot, e.g., in case of parallel parking, behind the parking slot with the heading parallel to the curb. They calculate the path of the parking maneuver based on geometric equations and do not take into account the obstacles in more complex environments.

In this paper, we overcome the above limitations by proposing a planning algorithm consisting of two phases that are executed in reverse order to the parking process itself. The phases are:

1. *In-slot planning* to find the so-called slot entry position and the path inside the slot. The path is calculated deterministically by a geometric planner.
2. *Out-of-slot planning* to calculate a collision-free path from an initial car position to the entry position found in the in-slot phase.

The particular contributions of this paper are:

- We formulate the parking problem differently from other authors. The goal parking position and the corresponding entry position are not explicitly given as inputs, but are the outputs of our *in-slot planner*. The in-slot planner has the location and size of the entire parking slot as inputs.

*<https://orcid.org/0000-0002-6618-8152>

†<https://orcid.org/0000-0002-8738-075X>

‡<https://orcid.org/0000-0002-8135-1296>

- We present several improvements to the Rapidly-exploring Random Trees (RRT) algorithm used by our *out-of-slot planner*: i) use of different metrics in different steps of the algorithm; a fast and inaccurate heuristic to find the nearest nodes, and a slower but accurate computation to find the cost of newly added nodes, ii) reuse of nodes from the previous iterations of the Anytime RRT algorithm, resulting in finding better paths faster.
- We introduce two concepts that are independent of RRT and improve the *out-of-slot planner*: i) we developed the goal zone concept, which allows us to efficiently compute the final condition of the search; many other authors use Euclidean distance as the final condition, which does not work well for non-holonomic vehicles, ii) we describe path optimization based on Dijkstra’s algorithm.
- We present the results of extensive computational experiments as well as experiments with a real Porsche Cayenne – see the video of the physical experiments at <https://youtu.be/u-Vqfd5Cn8Q>.

This paper is organized as follows. In Section 2, we formally define the parking problem. In Section 3, we introduce the in-slot planner. We describe enhancements of the RRT algorithm and propose the out-of-slot planner in Section 4. In Section 5, we evaluate our approach using both computational and physical experiments and discuss the results. The source code of our algorithm is publicly available¹.

1.1 Related Works

Automated driving, especially parking, has attracted a lot of attention in the last decade. The general architecture of automated cars is described by [Behere and Torngren \(2015\)](#). They divide the architecture into three main components: Perception, Decision and Control, and Vehicle Platform. According to their terminology, the main contribution of our

¹<https://rttime.ciirc.cvut.cz/gitweb/hubacji1/iamcar2.git>

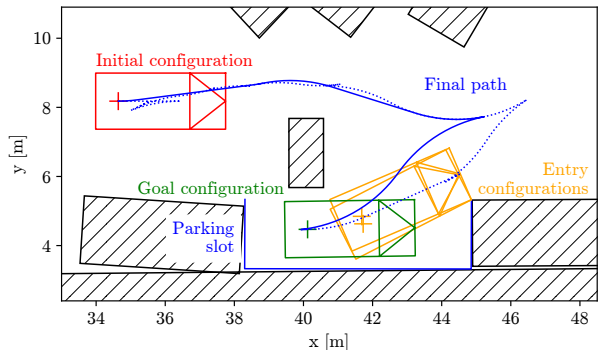


Figure 1: A real-world parking scenario. The black shaded objects are obstacles, the blue frame is the parking slot, the initial position is red, the entry positions are orange, and the goal position is green. The path before optimization is dotted in blue and the optimized final path is solid blue. The cross represents the center of the rear axle.

work is in the Decision and Control component. In addition, we dealt with the Vehicle Platform during the tests with the real vehicle.

State of the art in planning algorithms for automated vehicles is summarized by [González, Pérez, Milanés, and Nashashibi \(2016\)](#). The authors categorize planning algorithms into graph-search planners, sampling-based planners, interpolating curve planners, and planners based on numerical optimization. According to this classification, our in-slot planner falls into the category of interpolating curve planners (geometric planners), and our out-of-slot planner is a sampling-based planner.

In terms of automated parking, we divide related works into two groups. First, we compare our in-slot planner with planners used for maneuvering inside the parking slot. The second group deals with planners used outside the parking slot and focuses on sampling-based planners for non-holonomic vehicles.

1.1.1 In-slot planners

In-slot planners found in the literature can be divided into two classes: geometric planners ([M. H. Li & Tseng, 2016](#); [Petrov & Georgieva, 2018](#); [Voro-](#)

bieva, Glaser, Minoiu-Enache, & Mammar, 2015) and numerical optimization-based planners (Jing et al., 2018; B. Li, Wang, & Shao, 2016; Zips, Böck, & Kugi, 2016).

Planners of both classes often do not allow direction changes (Jing et al., 2018; M. H. Li & Tseng, 2016) or require that the goal position be specified precisely (Jing et al., 2018; Petrov & Georgieva, 2018; Vorobieva et al., 2015; Zips et al., 2016), which can lead to unnecessary direction changes.

Optimization planners are often slower than geometric planners (B. Li et al., 2016). However, with good heuristics, their performance can be sufficient for real-time (Zips et al., 2016).

The main difference between our in-slot planner and the above works is that our in-slot planner only requires the vehicle dimensions and the parking slot dimensions as input. The output includes the best position for entering the slot, the path in the slot, and the corresponding goal position. Thus, the goal position is the result and not the input. We have described our in-slot planner for parallel parking in more detail in our earlier work (Vlasak, Sojka, & Hanzálek, 2022).

1.1.2 Out-of-slot planners

Parking in unpredictable environments requires more sophisticated planning algorithms that can cover a larger area and take obstacles into account. Widely used algorithms for this task include graph-search planners, planners based on numerical optimization, and sampling-based planners. In recent years, planners using neural networks have gained prominence.

Optimization-based planners have the advantage of being able to describe kinematic, dynamic, or other complex constraints. However, to achieve acceptable performance for real-time use, various heuristics and simplifications must be used. For example, Zips et al. (2016) find the optimal path only between landmarks generated by the local optimization-based planner forming a tree. Conceptually, their approach is not very different from the RRT algorithm used in this work, since they use a random component in the placement of landmarks. Their planner has been successfully used by Jang et al. (2020) for fully

automated perpendicular parking. Similarly, Chi, Liu, Huang, Hong, and Su (2022) combine a graph search-based planner with a numerical optimization approach, where they first plan a rough, imprecise path that is then followed by a Model Predictive Controller.

Neural network-based planners suffer from several problems. End-to-end planners, such as that of Sousa, Ribeiro, Coelho, Lopes, and Ribeiro (2022), can only reliably park the vehicle within a finite distance (1.5 – 3 m) from the parking slot. The planner proposed by Liu, Li, Li, and Wang (2017) uses a neural network to find a smooth trajectory between two nearby points, but to find a path for longer distances, they still need a strategy to find so-called “middle/switching points”. Such a strategy can be provided, for example, by random or semi-random sampling.

As can be seen, sampling-based planners that include a random component still have an advantage in planning a path over a longer distance. Therefore, our out-of-slot planner is based on sampling. Sampling-based planners extend the set of sampled positions by attempting to connect to the positions (samples) they randomly generate. They can be tuned with different approaches to sample generation and can use arbitrary methods to connect samples. Although the planners are not deterministic, they are probabilistically complete and can be asymptotically optimal.

A classic sampling-based planning algorithm is the Rapidly-exploring Random Trees (RRT) algorithm (Lavalle, 1998). One of the first applications of RRT in the context of automated vehicles was developed by Kuwata, Fiore, Teo, Frazzoli, and How (2008). Several improvements to the RRT algorithm have been proposed, such as RRT-Connect by Kuffner and LaValle (2000), Dynamic RRT by Ferguson, Kalra, and Stentz (2006), or Anytime RRT by Ferguson and Stentz (2006). Karaman and Frazzoli (2011) have proposed RRT* – an asymptotically optimal variant of the RRT algorithm. Our out-of-slot planner is not asymptotically optimal, since we can also obtain good results with the plain RRT, as we explain later.

RRT is very popular in parking path plan-

ning (Dong, Zhong, & Hong, 2020; Feng, Chen, Chen, & Zheng, 2018; Jhang, Lian, & Hao, 2020; Wang, Jha, & Akemi, 2017). The planners described in the above papers differ mainly in the sampling strategy used and the extensions to the basic RRT algorithm. However, they also have many similarities. Since the paths generated by RRT are often crooked, most authors implement path smoothing as post-processing (Dong et al., 2020; Feng et al., 2018; Jhang et al., 2020). Similarly, many authors use Reeds-Shepp curves (Reeds & Shepp, 1990) at least in part of their algorithm (Dong et al., 2020; Jhang et al., 2020; Wang et al., 2017). Only Dong et al. (2020) validate the algorithm on a real vehicle.

In this paper, we propose several novel extensions to the RRT algorithm and show that the result can be successfully applied to a real vehicle.

In our previous work (Vlasak, Sojka, & Hanzálek, 2019), we extended the RRT*-based algorithm in a similar way; this work builds on the results of (Vlasak et al., 2019) but uses the plain RRT algorithm. In addition, we extend the parking algorithm with a multiphase approach and a goal zone concept, use an improved search cost heuristic, and apply Dijkstra’s optimization more efficiently. We also add more computational experiments to consider real-world scenarios and perform tests with a real vehicle, which is possible thanks to our previous experience (Záhora, Hanzálek, & Sojka, 2021).

2 The Parking Problem

In this section, we introduce the used terminology and formally define the parking problem.

2.1 Definitions

A car *configuration* is a tuple $C = (x, y, \theta, s, \phi)$, where x and y are Cartesian coordinates of the rear axle center in the global coordinate system and θ is car heading. To simplify our notation, we include the control input to car configuration; s is the control input of the direction $s \in \{-1, +1\}$, and ϕ is the steering angle $\phi \in [-\phi_{\max}, \phi_{\max}]$. Car configurations

are subject to a discrete kinematic model $C_{k+1} = f(C_k)$, $k \in \mathbb{N}$ where the function f is given by Eq. (1):

$$\begin{aligned} x_{k+1} &= x_k + s_k \cdot \Delta \cdot \cos(\theta_k) \\ y_{k+1} &= y_k + s_k \cdot \Delta \cdot \sin(\theta_k) \\ \theta_{k+1} &= \theta_k + \frac{s_k \cdot \Delta}{b} \cdot \tan(\phi_k), \end{aligned} \quad (1)$$

where $\Delta \in \mathbb{R}^+$ is a positive constant called the *step distance*. Fig. 1 shows the *initial*, *entry*, and *goal* configurations, which we denote by C_I , C_E , and C_G , respectively.

Car *dimensions* is a tuple $D = (w, d_f, d_r, b, \phi_{\max})$, where w is the width of the car, d_f and d_r are the distance from the rear axle center to the front and rear of the car, respectively, b is the wheelbase (distance between the front and rear axles), and ϕ_{\max} is the maximum steering angle.

A car *frame* $\mathcal{F}(C)$ is a rectangle given by the car configuration C and the car dimensions D . Figure 1 shows the car frame of the initial configuration in red. The red cross is centered at x, y , and the triangle inside the frame shows the car heading θ .

A *search space* Ω is a set of possible configurations $\Omega = \{C | x \in [x_{\min}, x_{\max}], y \in [y_{\min}, y_{\max}], \theta \in (-\pi, \pi], s \in \{-1, +1\}, \phi \in [-\phi_{\max}, \phi_{\max}]\}$ for some $x_{\min}, x_{\max}, y_{\min},$ and y_{\max} .

An *obstacle* is a convex polygon in \mathbb{R}^2 .

A *parking slot* is a rectangle that does not intersect with any obstacle and whose one side (called *entry side* in the following text) is adjacent to the road. The rectangle is defined as a tuple $P = (p, \delta, W, L)$, where the point $p \in \mathbb{R}^2$ is a corner of the rectangle on the entry side, δ is the direction of the entry side relative to p , see Fig. 3a, $W > w$ is the width of the parking slot, which is larger than the width of the car, and the length of the parking slot is $L \geq d_f + d_r$.

A *possible entry configuration* is a car configuration $C_E^P = (x, y, \theta)$ with the following properties: (i) the right front corner of the car frame $\mathcal{F}(C_E^P)$ coincides with the corner p of the parking slot, (ii) the car heading is between the angle parallel to the entry side and the angle perpendicular to the entry side, i.e., $\delta + \pi \leq \theta \leq \delta + 3/2\pi$, and (iii) the configuration frame $\mathcal{F}(C_E^P)$ does not intersect with non-entry sides

of the parking slot. We denote a set of possible entry configurations as \mathbf{C}_E^P and we can see an example subset of \mathbf{C}_E^P in Fig. 3a.

A *scenario* is a tuple $S = (\Omega, C_I, P, O)$, where Ω is a *search space* defined above, C_I is an initial configuration, P is a goal parking slot, and O is a set of obstacles.

A *path* \mathcal{P}_{C_1, C_M} from configuration C_1 to C_M is an ordered sequence of configurations (C_1, C_2, \dots, C_M) , where $C_{k+1} = f(C_k)$ for $k = 1, 2, \dots, M-1$ for a sequence of pairs $((s_1, \phi_1), (s_2, \phi_2), \dots, (s_{M-1}, \phi_{M-1}))$.

A *cost* $\mathcal{C}(C_1, C_2)$ between two configurations C_1 and C_2 is the length of the Reeds-Shepp curve between these configurations. A *path cost* $\mathcal{C}(\mathcal{P}_{C_1, C_M}) = \sum_{k=1}^{M-1} \mathcal{C}(C_k, C_{k+1})$.

We say that the configuration C *collides* when $\mathcal{F}(C)$ intersects with any obstacle of O .

A *feasible path* is one whose configurations do not collide.

2.2 Problem Statement

Our goal is to find a feasible path \mathcal{P}_{C_I, C_G} with a minimum number of backward-forward direction changes, where C_I is an initial configuration and the frame $\mathcal{F}(C_G)$ lies entirely within the parking slot P . Among all paths with minimum backward-forward direction changes, we search for the one with the lowest cost $\mathcal{C}(\mathcal{P}_{C_I, C_G})$ that can be found within a bounded computation time.

To find the solution more efficiently, we decompose the parking problem into two subproblems:

1. Finding the path inside the parking slot using a geometric approach. The geometric approach is preferable because the parking slot contains no obstacles and the constraints represented by the boundaries of the parking slot are simple. In addition to the path, we want to find a set of *entry configuration candidates* $\mathbf{C}_E \subset \mathbf{C}_E^P$ from which the car can park into the slot with a minimum number of direction changes.
2. The second subproblem is to find a feasible path \mathcal{P}_{C_I, C_E} from the initial configuration C_I to an entry configuration $C_E \in \mathbf{C}_E$ with the lowest path cost.

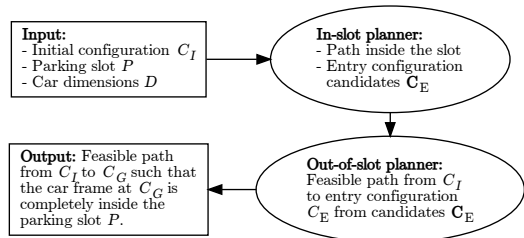


Figure 2: Data-flow diagram of our algorithm.

We solve the first subproblem with the so-called in-slot planner, described in Section 3, and the second with the out-of-slot planner, discussed in Section 4. The data-flow diagram is shown in Fig. 2.

3 In-slot Planner

This section describes our planning algorithm for finding a set of entry configuration candidates \mathbf{C}_E to a parking slot P and a corresponding path inside the slot for each $C_E \in \mathbf{C}_E$.

The input to the planner is the car dimensions tuple D and the parking slot P . Compared to related works presented in Section 1.1, our in-slot planner is unique in that it provides entry configuration candidates \mathbf{C}_E as output in addition to paths. We use entry configuration candidates as input to our out-of-slot planner described in Section 4.

We consider two different cases: Parallel parking and perpendicular parking. Parallel parking requires entering the slot only in backward direction, followed by backward-forward movements. Perpendicular parking, on the other hand, allows entering the slot in both directions and does not require backward-forward movements.

3.1 Parallel Parking

Our in-slot planner for parallel parking uses an approach similar to the “several reversed trials” planner of Vorobieva et al. (2015). Their planner assumes that the goal configuration C_G is known and starts with that configuration. Our in-slot planner starts with a set of possible entry configurations \mathbf{C}_E^P , some

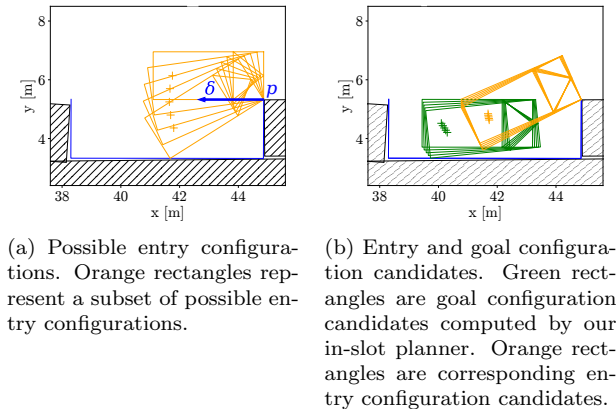


Figure 3: In-slot planner for parallel parking.

of them are shown as orange rectangles in Fig. 3a. For each possible entry configuration $C_E^P \in \mathbf{C}_E^P$, the in-slot planner simulates backward-forward movements with the maximum steering angle to find candidates for the goal configuration, shown as green rectangles in Fig. 3b.

The result of the in-slot planner for parallel parking is a series of paths from each entry configuration $C_E \in \mathbf{C}_E$, shown as orange rectangles in Fig. 3b, to the corresponding goal configuration candidate.

3.2 Perpendicular Parking

In perpendicular parking, the in-slot planner computes one entry configuration for the forward direction and one for the backward direction. Our in-slot planner first computes the goal configuration C_G , shown as a green rectangle in Fig. 4, such that for the forward (backward) direction, the rear (front) side of $\mathcal{F}(C_G)$ coincides with the entry side of the parking slot P . The entry configuration C_E , shown as an orange rectangle in Fig. 4, is computed by driving the car with the configuration C_G out of the parking slot P until the car can leave the slot with maximum steering.

The result of the in-slot planner for the perpendicular parking slot is the path \mathcal{P}_{C_E, C_G} from C_E to C_G for both directions.

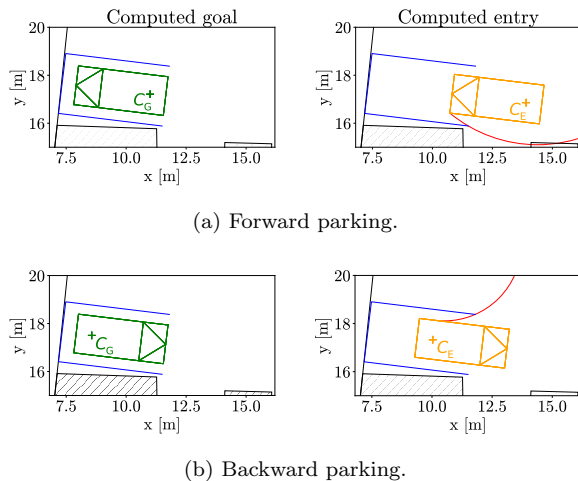


Figure 4: Forward (backward) perpendicular parking. On the left, there is computed goal configuration for the forward (backward) perpendicular parking. On the right, there is corresponding entry configuration. Red arcs represent path of front (rear) vehicle corners when moving backward (forward) with the maximum steering.

4 Out-of-slot Planner

Our out-of-slot planner for finding a feasible path \mathcal{P}_{C_I, C_E} from the initial to the entry configuration is based on the RRT algorithm extended with Dijkstra-based optimization. The pseudocode of our planner can be found in Alg. 1. FINDPATHRRT implements the RRT-based algorithm. We recall the original RRT algorithm in Section 4.1 and our improved version (FINDPATHRRT) in Section 4.2. Calling OPTIMIZE improves the path by skipping some configurations, as described in Section 4.3. These steps run several times in a loop, trying to improve the path cost in several iterations, taking advantage from the path found in the previous iteration. The algorithm stops when it reaches the maximum number of iterations I_{max} or the path returned by FINDPATHRRT has not improved in five iterations. We describe the implementation details in Section 4.4.

Compared to the RRT* algorithm (Karaman & Frazzoli, 2011), the RRT algorithm is not asymp-

totically optimal. However, when we apply the improvements introduced in this section to the RRT algorithm, the cost of the found paths is the same as when using RRT*, but the performance is slightly better due to omitting the rewire procedure of the RRT*.

Algorithm 1 Out-of-slot planner

- Input: C_I , entry conf. candidates C_E , obstacles O .
- Output: Feasible path \mathcal{P}_{C_I, C_E} from C_I to $C_E \in C_E$.

```

1:  $\mathcal{P}_{C_I, C_E} \leftarrow ()$   $\triangleright$  no path, therefore  $\mathcal{C}(\mathcal{P}_{C_I, C_E}) \leftarrow \infty$ 
2:  $noImprovementCounter \leftarrow 0$ 
3:  $i \leftarrow 0$   $\triangleright$  number of iterations
4: while  $i < I_{max} \wedge noImprovementCounter < 5$ 
   do
5:    $\mathcal{P}_{prev} \leftarrow \mathcal{P}_{C_I, C_E}$ 
6:    $path, i \leftarrow \text{FINDPATHRRT}(C_I, C_E, O, i, \mathcal{P}_{prev})$ 
7:   if  $\mathcal{C}(path) < 1.25 \cdot \mathcal{C}(\mathcal{P}_{C_I, C_E})$  then
8:      $path \leftarrow \text{OPTIMIZE}(path)$ 
9:   end if
10:  if  $\mathcal{C}(path) < \mathcal{C}(\mathcal{P}_{C_I, C_E})$  then
11:    if  $\mathcal{C}(path) < 0.75 \cdot \mathcal{C}(\mathcal{P}_{C_I, C_E})$  then
12:       $noImprovementCounter \leftarrow 0$ 
13:    end if
14:     $\mathcal{P}_{C_I, C_E} \leftarrow path$ 
15:  else
16:    Increment  $noImprovementCounter$ 
17:  end if
18: end while
19: return  $\mathcal{P}_{C_I, C_E}$ 

```

4.1 Original RRT

Rapidly-Exploring Random Trees (RRT) (Lavalle, 1998) is a randomized algorithm for searching a state space. The RRT-based algorithms can be used for solving path planning problems, such as our parking problem defined in Section 2.2.

The RRT algorithm uses a tree data structure. The algorithm can handle nonholonomic constraints, ar-

bitrary obstacles, and constraints on configurations. Therefore, the RRT is suitable for solving real-world scenarios.

We denote the tree data structure as $\mathcal{T} = (C_I, V, E)$, where C_I is the root of the tree and V is a set of configurations. The set of edges E maintains the parent-child relationship between the configurations such that $(C_i, C_j) \in E \Leftrightarrow C_i, C_j \in \mathcal{P}_{C_I, C_M} = (C_I, \dots, C_i, C_j, \dots, C_M)$. We can see the pseudocode of the original RRT in Alg. 2.

Algorithm 2 Original RRT

- Input: C_I , obstacles O .
- Output: \mathcal{T} data structure representing feasible paths between configurations $C \in \Omega \cap \mathcal{T}$

```

1: Initialize the tree  $\mathcal{T} = (C_I, \emptyset, \emptyset)$ 
2: while number of iterations  $< I_{max}$  do
3:    $RC \leftarrow \text{RANDOMCONFIGURATION}()$ 
4:    $NN \leftarrow \text{NEARESTNEIGHBOR}(\mathcal{T}, RC)$ 
5:    $C_N \leftarrow \text{STEER}(NN, RC)$ 
6:   if  $\text{COLLIDES}(C_N, O)$  then
7:     continue the while loop
8:   end if
9:    $\text{CONNECT}(\mathcal{T}, NN, C_N)$ 
10: end while

```

4.2 RRT Enhancements

In this section, we describe our enhancements to the original RRT algorithm that allow us to find a path between C_I and C_E more efficiently. The pseudocode of the RRT-based FINDPATHRRT procedure can be found in Alg. 3. Individual enhancements are described in the following subsections.

4.2.1 Reuse of Previous Paths with Anytime RRT

Our algorithm uses the random sampling procedure shown in Alg. 4, which is inspired by the Anytime RRT (Ferguson & Stentz, 2006) algorithm. However, instead of repeating random sampling when $RC_{cost}^1 + RC_{cost}^2 > \mathcal{C}(\mathcal{P}_{prev})$, we return a randomly

chosen configuration from the previously found path $\mathcal{P}_{\text{prev}}$, likely leading to its improvement.

Algorithm 3 RRT for finding a path

```

1: procedure FINDPATHRRT( $C_I, \mathbf{C}_E, O, i, \mathcal{P}_{\text{prev}}$ )
2:   Initialize the tree  $\mathcal{T} = (C_I, \emptyset, \emptyset)$ 
3:   while  $i < I_{\text{max}}$  do
4:      $i \leftarrow i + 1$ 
5:     if  $i == 1$  then
6:        $RC \leftarrow C_E$ 
7:     else
8:        $RC \leftarrow$ 
RANDOMCONFIGURATION( $\mathcal{P}_{\text{prev}}$ )
9:     end if
10:     $NN \leftarrow$  NEARESTNEIGHBOR( $RC$ )
11:     $\mathcal{P}_{NN,RC} \leftarrow$  STEERPATH( $NN, RC$ )
12:     $\mathcal{P}_{NN,CF} \leftarrow$ 
REMOVECOLLIDING( $\mathcal{P}_{NN,RC}, O$ )
13:    if  $\mathcal{P}_{NN,CF} = \emptyset$  then
14:      continue the while loop
15:    end if
16:    CONNECT( $\mathcal{T}, \mathcal{P}_{NN,CF}$ )
17:    STEERTOWARDENTRY( $\mathcal{P}_{NN,CF}, \mathbf{C}_E$ )
18:    if some  $C_E \in \mathbf{C}_E$  added to  $\mathcal{T}$  then
19:      Find  $\mathcal{P}_{C_I, C_E}$  in  $\mathcal{T}$ 
20:      return  $\mathcal{P}_{C_I, C_E}, i$ 
21:    end if
22:  end while
23: end procedure

```

4.2.2 Cost Heuristic for Nearest Neighbor Search

The original RRT algorithm (Alg. 2) uses the cost function \mathcal{C} in two places: (i) within the NEARESTNEIGHBOR search (Line 4.) and (ii) when connecting new nodes (Line 9).

From the analysis of the original RRT, we see that it computes the cost \mathcal{C} more often when searching the tree than when connecting. The difference in the number of these cases is greater the larger the tree is. If we manage to speed up the cost calculation in NEARESTNEIGHBOR, we can improve the total computation time significantly.

Algorithm 4 Random sampling

```

1: procedure RANDOMCONFIGURATION( $\mathcal{P}_{\text{prev}}$ )
2:    $RC \leftarrow$  random sample from  $\Omega$ 
3:    $RC_{\text{cost}}^1 \leftarrow$  SEARCHCOST( $C_I, RC$ )
4:    $RC_{\text{cost}}^2 \leftarrow$  SEARCHCOST( $RC, C_E$ )
5:   if  $RC_{\text{cost}}^1 + RC_{\text{cost}}^2 > \mathcal{C}(\mathcal{P}_{\text{prev}})$  then
6:      $RC \leftarrow$  random configuration from  $\mathcal{P}_{\text{prev}}$ 
7:   end if
8:   return  $RC$ 
9: end procedure

```

Therefore, our NEARESTNEIGHBOR search, uses the K-d tree data structure and computes the cost approximately by applying the heuristic \mathcal{C}' in Eq. (2), which we found to be most suitable for our purposes. \mathcal{C}' estimates the cost of path between configurations $C_{\mathcal{T}} = (x_{\mathcal{T}}, y_{\mathcal{T}}, \theta_{\mathcal{T}}) \in \mathcal{T}$ and $C_{RC} = (x_{RC}, y_{RC}, \theta_{RC})$ as:

$$\mathcal{C}' = \max \left(\Delta_E, \Delta_A \cdot \frac{b}{\tan \phi_{\text{max}}} \right) + 0.1 \cdot \Delta_{\text{BF}}, \quad (2)$$

where b and ϕ_{max} are given by car dimensions and the other elements are the following simple functions: $\Delta_E = \sqrt{(y_{RC} - y_{\mathcal{T}})^2 + (x_{RC} - x_{\mathcal{T}})^2}$ is the Euclidean distance, $\Delta_A = \min(|\theta_{RC} - \theta_{\mathcal{T}}|, 2 \cdot \pi - |\theta_{RC} - \theta_{\mathcal{T}}|)$ is the angular difference, and Δ_{BF} is the cumulative number of backward-forward directions changes between C_I and $C_{\mathcal{T}}$.

We use the cost heuristic only when searching the tree for the nearest neighbor in Line 10 in Alg. 3. We use the length of the Reeds-Shepp curve, which satisfies the kinematic constraints when we connect new nodes in Line 9. Therefore, the paths in the tree also satisfy the kinematic constraints.

4.2.3 Steering and Collision Checking

The original RRT algorithm extends the tree only by one configuration per iteration and therefore the tree grows slowly. Moreover, in the original RRT algorithm, the tree grows uniformly in all directions, but for our problem, it is advantageous if the growth is directed toward the goal.

To make the tree grow faster, we add multiple configurations in one iteration by replacing the STEER procedure with STEERPATH, which returns a path between the random configuration and its nearest node in the tree. All the configurations in path before the first obstacle (if any, see Alg. 5) are added to the tree.

Algorithm 5 Collision check

```

1: procedure REMOVECOLLIDING( $\mathcal{P}_{\text{NN,RC}}, O$ )
2:    $\text{CF} \leftarrow \text{NN}$ 
3:   for  $C_N \in \mathcal{P}_{\text{NN,RC}}$  do
4:     if COLLIDES( $C_N, O$ ) then
5:       return  $\mathcal{P}_{\text{NN,CF}}$ 
6:     end if
7:      $\text{CF} \leftarrow C_N$ 
8:   end for
9: end procedure

```

To direct the growth of the tree toward the entry configurations \mathbf{C}_E , we try to construct Reeds-Shepp path from each added configuration to an entry configuration and add all their configurations before the potential collision. This is implemented in STEERTOWARDENTRY as detailed in Alg. 6. This improvement was originally proposed by Kuwata et al. (2008).

4.2.4 Goal Zone

To decide whether we have found the complete path, i.e., whether the constructed tree \mathcal{T} contains an entry configuration $C_E \in \mathbf{C}_E$, we introduce the concept of *goal zone* and use it in Line 10 in Alg. 6.

The *goal zone* \mathbf{G} of an entry configuration C_E and heading θ_G is the set of configurations C_g , where $\theta_g = \theta_G$ and the configuration C_E is trivially reachable from C_g by a line segment, an arc with maximum steering radius, and a subsequent line segment. Furthermore, we consider the goal zone to be empty if $|\theta_G - \theta_E| \geq \frac{\pi}{2}$. We see an example of a goal zone \mathbf{G} in Fig. 5.

4.3 Path Optimization

It is well known that the RRT algorithm is unlikely to converge to the optimal solution. Although the

Algorithm 6 Steering toward the entry configuration

```

1: procedure STEERTOWARDENTRY( $\mathcal{P}_{\text{NN,CF}}, \mathbf{C}_E$ )
2:    $C_E^{\text{avg}} \leftarrow$  average of  $\mathbf{C}_E$ 
3:   for  $C_k \leftarrow \mathcal{P}_{\text{NN,CF}}$  do
4:      $\mathcal{P}_{C_k, C_E} \leftarrow$  STEERPATH( $C_k, C_E^{\text{avg}}$ )
5:      $\mathcal{P}_{C_k, \text{CF}}$  ←
6:     REMOVECOLLIDING( $\mathcal{P}_{C_k, C_E}, O$ )
7:     if  $\mathcal{P}_{C_k, \text{CF}} = \emptyset$  then
8:       continue the for loop
9:     end if
10:    CONNECT( $\mathcal{T}, \mathcal{P}_{C_k, \text{CF}}$ )
11:    if  $\text{CF} \in \mathbf{G}(\mathbf{C}_E, \theta_{\text{CF}}) \wedge |\text{CF} - C_E| \leq \Delta$ 
12:      then
13:        Add corresponding  $C_E$  to the tree  $\mathcal{T}$ 
14:      end if
15:    end for
16: end procedure

```

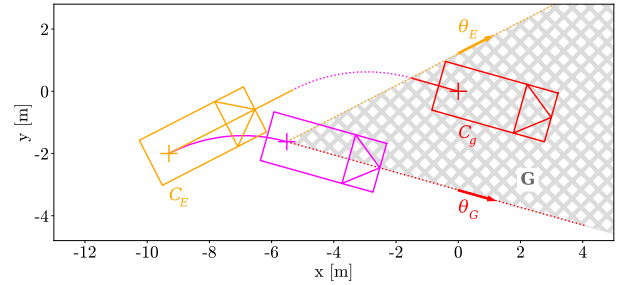


Figure 5: Goal Zone \mathbf{G} . C_E is trivially reachable from C_g .

RRT* is asymptotically optimal, it converges to the optimal solution very slowly. Depending on the scenario, a feasible path returned by the algorithms may be hundreds of percent away from the optimum.

To accelerate convergence to the optimal solution, we introduce path optimization based on Dijkstra's shortest path algorithm. The path optimization algorithm is applicable to both RRT and RRT*. Recall that we use RRT.

The optimization works as follows. Given a path \mathcal{P}_{C_i, C_E} , we find a set of its *interesting configurations*. An *interesting configuration* C_i is either (i) first or

last configuration in the path, (ii) a configuration with a change in the direction of motion, or (iii) given an interesting configuration C_i , the last configuration C_j in its goal zone is also an interesting configuration, i.e., $C_j \in \mathbf{G}(C_i, \theta_j) \wedge C_{j+1} \notin \mathbf{G}(C_i, \theta_{j+1})$ where $i < j$ and j is the smallest value satisfying the condition.

We run Dijkstra’s algorithm on the directed graph, where the vertices of the graph represent the interesting configurations. Edges are created between two interesting configurations C_i, C_j if and only if $i < j \wedge C_j \in \mathbf{G}(C_i, \theta_j) \wedge \text{STEERPATH}(C_i, C_j)$ is feasible. The cost of the edge is $\mathcal{C}(C_i, C_j)$. Running Dijkstra’s algorithm finds a new feasible path from C_I to C_E , possibly skipping some *interesting configurations*.

We perform path optimization in both directions, as we can see in Alg. 7. An example of a path before and after optimization can be found in Fig. 1.

4.4 Implementation

In this section, we provide information about the implementation.

We generate random configurations in RANDOMCONFIGURATION by selecting it with uniform distribution from the circular subspace $\Omega_C \subseteq \Omega$. $\Omega_C = \{C | (x - x_C)^2 + (y - y_C)^2 \leq R^2, \theta \in (-\pi, \pi]\}$, where x_C and y_C are Cartesian coordinates of the center of the line segment from C_I to C_E , and R is the length of the line segment from C_I to C_E . (The diameter of the circular subspace is twice the distance from C_I to C_E .)

We use the OMPL (Sucan, Moll, & Kavraki, 2012) implementation of the optimal paths of Reeds and Shepp (1990) for the STEER and STEERPATH procedures. The distance between the configurations of a path returned by STEERPATH is 0.5 m.

To find the NEARESTNEIGHBOR and NEARNODES, we use a 3D K-d tree structure.

For collision detection in the COLLIDES and REMOVECOLLIDING procedures, we use the GJK algorithm from *cute_headers* library (RandyGaul & Wizard033, 2019).

We terminate the out-of-slot planner at the iteration limit or when the path cost has not improved in five consecutive algorithm resets.

Algorithm 7 Path optimization

```

1: procedure OPTIMIZE( $\mathcal{P}_{C_I, C_E}$ )
2:   while  $\mathcal{C}(\mathcal{P}_{C_I, C_E})$  is improving do
3:      $\mathbf{I} \leftarrow \text{INTERESTINGCONFIGURATIONS}(\mathcal{P}_{C_I, C_E})$ 
4:     Run Dijkstra on  $\mathbf{I}$  starting from  $C_I$ 
5:     Update  $\mathcal{T}$  with the new feasible path
6:      $\mathcal{P}_{C_I, C_E} \leftarrow \text{reverse } \mathcal{P}_{C_I, C_E}$ 
7:      $\mathbf{I} \leftarrow \text{INTERESTINGCONFIGURATIONS}(\mathcal{P}_{C_E, C_I})$ 
8:     Run Dijkstra on  $\mathbf{I}$  starting from  $C_E$ 
9:     Update  $\mathcal{T}$  with the new feasible path
10:  end while
11:  return  $\mathcal{P}_{C_I, C_E}$ 
12: end procedure
13: procedure INTERESTINGCONFIGURATIONS( $\mathcal{P}_{C_1, C_2}$ )
14:    $C_i \leftarrow C_1$ 
15:   while  $C_i \neq C_2$  do
16:      $\mathbf{I} \leftarrow (C_i)$ 
17:     Find the first  $C_j : j > i \wedge C_{j+1} \notin \mathbf{G}(C_i, \theta_{j+1})$ 
18:      $\mathbf{I} \leftarrow \mathbf{I} \cup (C_k | i < k < j \wedge s \text{ of } C_k \text{ has changed})$ 
19:      $\mathbf{I} \leftarrow \mathbf{I} \cup (C_j)$ 
20:      $C_i \leftarrow C_j$ 
21:   end while
22:    $\mathbf{I} \leftarrow \mathbf{I} \cup (C_2)$ 
23:   return  $\mathbf{I}$ 
24: end procedure

```

The algorithms are written in C++. We use the *jsoncpp* library to read scenario definitions and write the results.

5 Experiments and Evaluation

In this section we show the results of the algorithm. We start with the computational experiments. We evaluate the combination of in-slot and out-of-slot planners in simple scenarios in Section 5.1, in real-world scenarios in Section 5.2, and in real-world scenarios with artificial obstacles in Section 5.3. Finally, we report results of physical experiments with Porsche Cayenne in Section 5.4.

The RRT-based out-of-slot planner incorporates the enhancements presented in this paper, i.e., cost heuristic, goal zone, and path optimization, as well as other well-known enhancements, namely, Anytime RRT, K-d tree, and steering toward the goal. To evaluate our contribution, we need to distinguish between these our and well known enhancements. Therefore, we refer to the out-of-slot planner with all the improvements as *OSP-All* and the out-of-slot planner with only the well-known improvements as *OSP-WK*.

For our computational experiments, we use the vehicle dimensions of the Renault Zoe from [Vorobieva et al. \(2015\)](#): $w = 1.625$ m, $d_f = 3.105$ m, $d_r = 0.655$ m, $b = 2.450$ m, and $\phi_{\max} = 31.4^\circ$, which gives the diameter of the turning circle (curb to curb) of the car 10.820 m. The maximum number of iterations of the out-of-slot planner is $I_{\max} = 1000$.

We run the computational experiments on a single core of Intel(R) Core(TM) i7-5600U CPU @2.60 GHz with 16 GB RAM.

5.1 Simple Scenarios

We test our planners on 1000 randomly generated *simple scenarios*, generated as follows: The initial configuration is $C_1 = (0, 0, 0)$. The parking slot is parallel or perpendicular with equal probability and is located at a random position 20 m from C_1 . There are eight square obstacles with an edge length of 2 m randomly positioned within 20 m of C_1 .

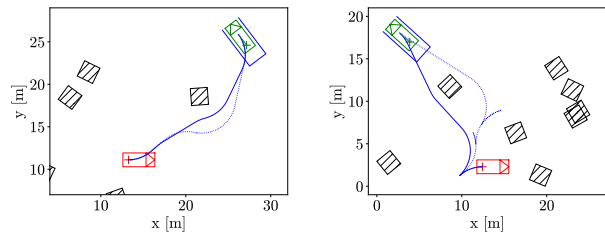


Figure 6: Details of the simple parking scenarios. The color legend is the same as in Fig. 1.

In Fig. 6 we can see the examples of simple parking scenarios and the solutions of our planners. Also, we can see the idea of path optimization – the difference between the solid (optimized) path and the dotted (original) path. We conclude that the resulting optimized paths are close to paths that would be driven by a human driver.

5.2 Real-world Scenarios

We test our planners on four real-world scenarios created from the orthophoto map of Prague streets (*Ortofoto Archiv*, n.d.). The detailed layouts of the real-world parking scenarios can be found in Fig. 7.

We run the out-of-slot planner 10 000 times for each scenario. The computation times measured on our hardware for the in-slot planner and the out-of-slot planner, as well as the final path costs after optimization, can be found in Table 1.

For more information on how the algorithm works for Scenario 3, the scenario with the longest computation time, see Figs. 8 to 10. Figure 8 shows the distribution of the final path cost (including optimization) after each iteration of the algorithm. We see that the cost does not change in the last third of iterations. From the drop of failure rate to zero, we can also see that the path is always found at least after 271 iterations.

In Figs. 9 and 10, we show evolution of failure rate and the average final path cost and compare them for different settings of our out-of-slot planner. There, *OSP-WK* denotes the results for the out-of-slot planner with only the well-known improvements, i.e., Alg. 1 without cost heuristic, goal zone, and path

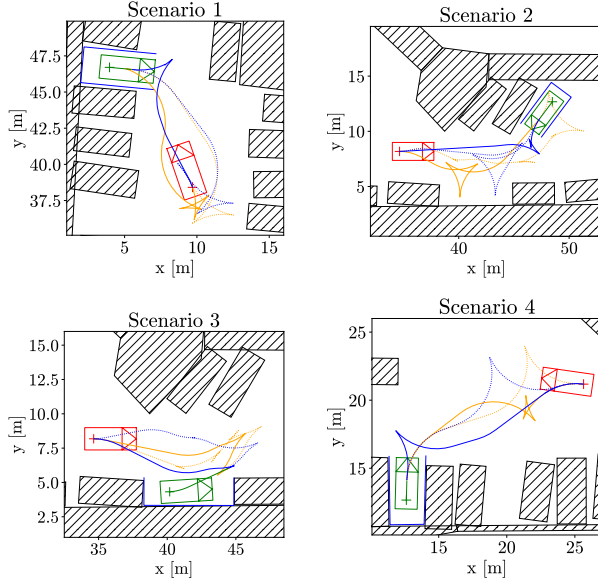


Figure 7: Details of the real-world parking scenarios. The color legend is the same as in Fig. 1. Additionally, orange indicates the worst path found.

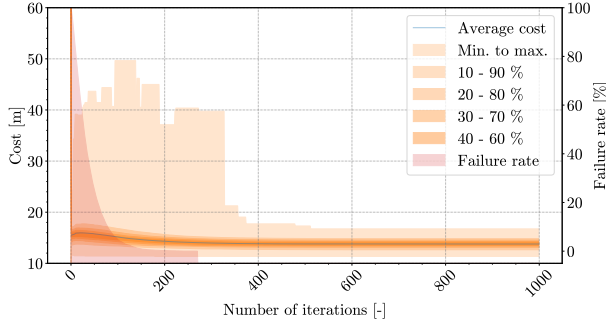


Figure 8: Evolution of final path cost after optimization for Scenario 3. The orange area shows the path cost after optimization. The red horizontal line is the average path cost after optimization. The red area shows how many planner runs failed to find the path for the scenario.

optimization. We also show the results of the planner using only one of our enhancements in isolation, that is: the cost heuristic, goal zone, and path optimization.

Table 1: Real-world parking scenarios results.

| Scenario | 1 | 2 | 3 | 4 |
|--|-------------|-------------|------------|-------------|
| In-slot planner computation time | | | | |
| Maximum [ms] | ≈ 0 | ≈ 0 | 19 | ≈ 0 |
| Maximum computation time (plus time of the optimization) | | | | |
| OSP-All [ms] | 297 + 64 | 920 + 83 | 1 416 + 58 | 452 + 124 |
| OSP-WK [ms] | 3 020 | 8 258 | 22 118 | 1 768 |
| Average computation time (plus time of the optimization) | | | | |
| OSP-All [ms] | 131 + 2 | 406 + 8 | 611 + 6 | 209 + 4 |
| OSP-WK [ms] | 685 | 3 310 | 9 762 | 486 |
| Improved by | 81% | 87% | 94% | 56% |
| Maximum final path cost (after optimization) | | | | |
| OSP-All [m] | 21.96 | 26.00 | 16.74 | 22.55 |
| OSP-WK [m] | 26.02 | 62.03 | 82.50 | 32.01 |
| Average final path cost (after optimization) | | | | |
| OSP-All [m] | 15.93 | 21.88 | 13.78 | 20.12 |
| OSP-WK [m] | 18.91 | 25.89 | 27.09 | 20.99 |
| Improved by | 16% | 15% | 49% | 4% |
| Minimum number of iterations when a path is found in 100% of cases | | | | |
| OSP-All [-] | 59 | 353 | 271 | 43 |
| OSP-WK [-] | 365 | - | - | 120 |
| Improved by | 84% | - | - | 64% |

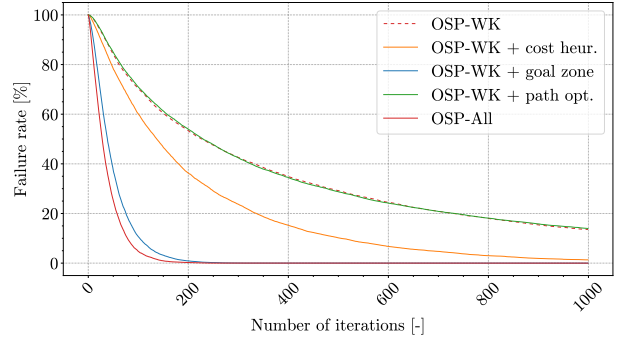


Figure 9: Evolution of failure rate for Scenario 3.

tion. Finally, we show the results for the out-of-slot planner with all of our enhancements combined, denoted as OSP-All.

In Fig. 9, we can see that the cost heuristic and the goal zone concept lower the failure rate. The cost heuristic lowers the failure rate from 14% to 1.32% in the 1000th iteration. The goal zone ensures that a path is found 100% of the time after at least 399 iterations. When used together (OSP-All), a path is found 100% of the time after at least 271 iterations for Scenario 3. For comparison, the failure rate for OSP-WK is 45% in the same iteration. The path optimization has no influence on the failure rate because

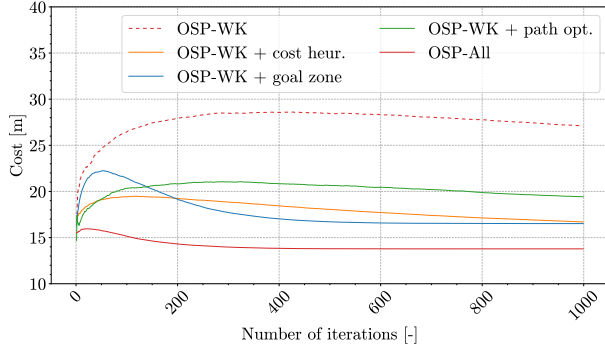


Figure 10: Evolution of average final path cost for Scenario 3.

it is executed only after the path has been found.

In Fig. 10, we can see that the cost heuristic and the goal zone improve the final path cost. This is the secondary effect of the improved failure rate – a path is found in fewer iterations and the algorithm is reset to find another path that can improve the current best path. As we can see at the last iteration, the cost heuristic improves the final path cost by 38%, the goal zone by 39%. Next, path optimization improves the found path by skipping parts of it, which leads to 28% enhancements at the last iteration. When combining all enhancements, the average final path cost for Scenario 3 improves by 49%.

5.3 Real-world Scenarios with Artificial Obstacles

To demonstrate the performance of our planners in constrained environments, i.e., the environments, where traditional geometric planners fail, we extend the real-world scenarios with artificial obstacles. Fig. 11 shows the detailed layouts of the extended scenarios. The solutions shown in Fig. 11 are close to the paths that a human driver would choose.

The computation times measured on our hardware for the in-slot planner and the out-of-slot planner, as well as the final path costs after optimization, can be found in Table 2.

Scenarios 5 and 6 extend Scenario 3 from Section 5.2. We can see that Scenario 3 requires fewer

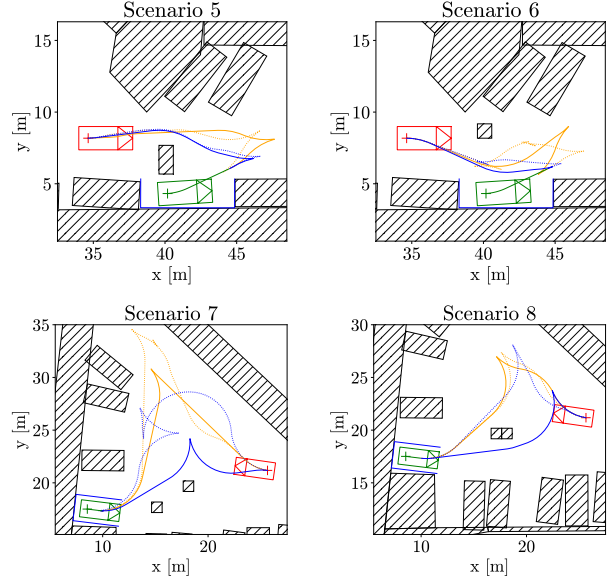


Figure 11: Details of the real-world parking scenarios with artificial obstacles. The color legend is the same as in Fig. 1. Additionally, orange indicates the worst path found.

iterations to find a path with 100% probability. On the other hand, Scenarios 5 and 6 are solved in less time compared to Scenario 3. This is due to reduction of search space size.

Scenarios 7 and 8 are based on a scenario that, in the absence of artificial obstacles, can be trivially solved using Reeds-Shepp geometric planner. With the addition of the obstacles, the scenarios become more difficult to solve. However, our algorithm finds a good path in an acceptable time of at most 3.5 s.

5.4 Experiments with a Real Vehicle

To validate our algorithm in practice, we conducted parking experiments with a Porsche Cayenne GTS V8 vehicle (Fig. 12) controlled via FlexRay from our external computer without any obstacle detection system. We prepared two scenarios with a parking slot and artificially placed obstacles. For each scenario, we manually created a description of the scene that served as input to our planning algorithm and let the

Table 2: Real-world parking scenarios with artificial obstacles results.

| Scenario | 5 | 6 | 7 | 8 |
|--|------------|------------|-------------|-------------|
| In-slot planner computation time | | | | |
| Maximum [ms] | 20 | 19 | ≈ 0 | ≈ 0 |
| Maximum computation time (plus time of the optimization) | | | | |
| OSP-All [ms] | 885 + 51 | 1 382 + 48 | 2 868 + 712 | 1 244 + 244 |
| OSP-WK [ms] | 8 733 | 11 096 | 10 391 | 4 906 |
| Average computation time (plus time of the optimization) | | | | |
| OSP-All [ms] | 421 + 3 | 559 + 5 | 1 372 + 32 | 567 + 32 |
| OSP-WK [ms] | 5 244 | 7 087 | 6 376 | 874 |
| Improved by | 92% | 92% | 78% | 31% |
| Maximum final path cost (after optimization) | | | | |
| OSP-All [m] | 17.35 | 17.61 | 31.38 | 25.28 |
| OSP-WK [m] | 75.01 | 72.55 | 76.03 | 30.03 |
| Average final path cost (after optimization) | | | | |
| OSP-All [m] | 15.31 | 13.67 | 22.96 | 21.11 |
| OSP-WK [m] | 24.70 | 26.89 | 32.77 | 22.52 |
| Improved by | 38% | 49% | 30% | 6% |
| Minimum number of iterations when a path is found in 100% of cases | | | | |
| OSP-All [-] | 393 | 392 | 464 | 51 |
| OSP-WK [-] | - | - | - | 335 |
| Improved by | - | - | - | 85% |



Figure 12: Porsche Cayenne testing the paths produced by our planning algorithm.

algorithm compute the parking path. Then we followed the path in three runs by car and evaluated the difference between the planned and the actual goal configuration. A video of the experiments can be found at <https://youtu.be/u-Vqfd5Cn8Q>.

The car was controlled by the software based on the Robot Operating System (ROS) version 2 (*Robot Operating System*, 2023). The path-following algorithm used only signals available from the onboard FlexRay busses. The vehicle was also equipped with an external differential GPS that receives NTRIP corrections and was used only to record the vehicle trajectory for evaluation. The accuracy of the GPS was reported to be less than 1 cm for position and 1° for heading.

To follow the path of our planning algorithm, we divide it into one or more segments; at the end of each segment, the car stops. The segments end at cusp points where the direction of the path changes, and at inflection points where the sign of the path curvature changes, if both surrounding arcs are longer than 1 m. Each segment is then followed with trapezoidal speed profile. A path segment is represented by function $\text{seg} : l \rightarrow (v, \phi, \theta)$, which returns the velocity v , the steering angle ϕ , and the expected heading θ based on the length l from the beginning of the path segment. In the following, the velocity component of this function is abbreviated as $v(l)$ and the other components are abbreviated analogously.

We control the car with two independent controllers running at 50 Hz, one for longitudinal and one for lateral movements. Both receive the data from the odometry of the car. Specifically, the distance traveled, l , is calculated as the cumulative sum of the average speed v_r of the rear wheels, which is reported by the ESP ECU. The heading of the vehicle θ is made available a signal generated by the EML ECU. Since this signal does not drift in time, we assume that the vehicle computes it by fusing data from odometry and the internal GPS. The longitudinal P controller computes the acceleration demand $a_{\text{dem}} = v(l)' + P_v(v_r - v(l))$, where $v(l)'$ is the time derivative of the reference velocity signal and P_v is the P constant of the controller. The lateral P controller calculates the steering angle demand $\phi_{\text{dem}} = \text{rlim}(\phi(l) + P_\theta(\theta - \theta(l)))$, where P_θ is the P constant of the controller and rlim is a rate limit-

ing function that prevents sending big steps in the demand to the vehicle steering controller.

The data obtained from two scenarios of the physical experiments are shown in Figs. 13 and 14 with the actual position measured by external GPS in three runs for each scenario. In the simpler experiment with only one direction change (Fig. 13), the vehicle followed the path very closely and the final vehicle positions were always within 10×10 cm of the planned goal position. In the more complex scenario with four direction changes (Fig. 14), the final positions were within 15×40 cm of the planned goal position. The higher inaccuracy occurs in the longitudinal direction. This is because the car responds to the a_{dem} signal with a delay, as can be seen from the velocity plot. We believe that the delay would be shorter and the inaccuracy would be lower if the controller was running in the parking ECU and not in our external computer. Nevertheless, even in this complex scenario, the car was always able to park and avoid obstacles.

6 Conclusion

In this paper, we proposed a planning algorithm for automated vehicle parking. The algorithm can deal with detected obstacles and its output is a path that the vehicle control system, such as the one described in this paper, could follow. The algorithm includes two different planners for different phases of the parking process. The in-slot planner provides the candidate entry position and maneuver inside the parking slot. Then, the RRT-based out-of-slot planner computes a drivable, collision-free, near-optimal path from the initial position to a candidate entry position.

Compared to other RRT-based planners, our algorithm provides the following improvements: (1) the parking position is given by the coordinates of the whole parking slot instead of just a single point, (2) the use of different heuristics in the search and build phases of the RRT algorithm, (3) the reuse of past paths in the Anytime RRT, (4) the concept of goal zone to check whether the RRT algorithm has reached the goal, and (5) the path optimization based on Dijkstra’s shortest path algorithm.

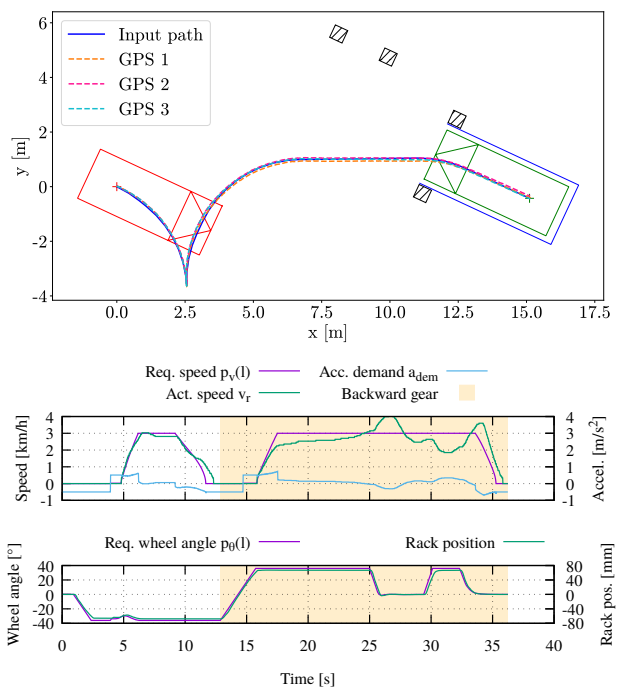


Figure 13: Simple physical experiment – perpendicular parking with one direction change.

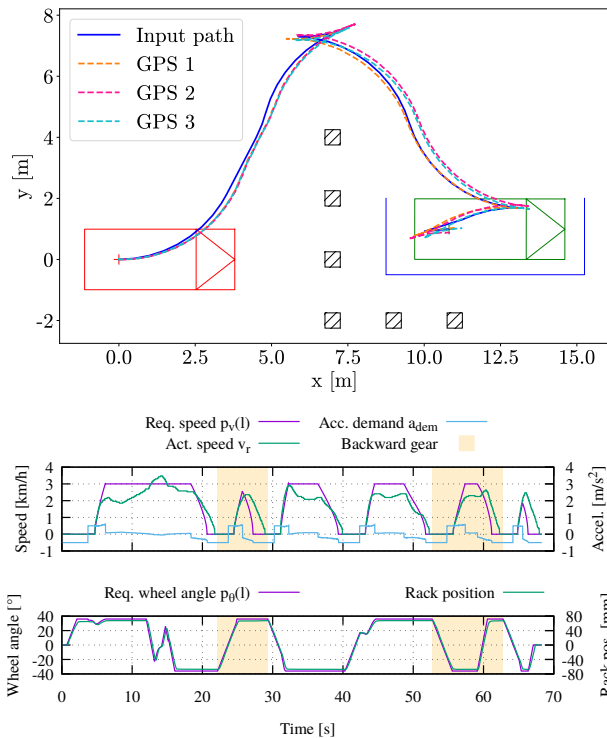


Figure 14: Complex physical experiment – parallel parking with four direction changes.

By using the cost heuristic, the goal zone, and the path optimization, the number of iterations required to achieve a zero error rate is reduced by 74 %. Similarly, the final path cost is improved by 21 % on average and the computation time is improved by 79.5 %. Our algorithm results in paths similar to those human drivers would drive themselves, which has been confirmed in physical experiments with the Porsche Cayenne.

The limitations of our algorithm arise from the fact that the path is composed of Reeds-Shepp curves. That is: the path curvature is discontinuous and uses only the maximum steering angles. In our future work, we intend to address these limitations by using a different interpolation algorithm for the final path optimization. The RRT algorithm, where each iteration must be fast, will continue to use simple Reeds-Shepp curves. We would also like to improve the performance of our algorithm by replacing uniform sampling with more targeted sampling.

Acknowledgement(s)

This work was supported by the Grant Agency of the Czech Technical University in Prague, grant No. SGS22/167/OHK3/3T/13.

References

- Behere, S., & Torngren, M. (2015, May). A functional architecture for autonomous driving. In *Proc. First Int. Workshop Automotive Software Architecture (WASA)* (pp. 3–10).
- Chi, X., Liu, Z., Huang, J., Hong, F., & Su, H. (2022, October). *Optimization-Based Motion Planning for Autonomous Parking Considering Dynamic Obstacle: A Hierarchical Framework*. arXiv. Retrieved 2023-01-02, from <http://arxiv.org/abs/2210.13112> (arXiv:2210.13112 [cs])
- Dong, Y., Zhong, Y., & Hong, J. (2020). Knowledge-Biased Sampling-Based Path Planning for Automated Vehicles Parking. *IEEE Access*, 8,

- 156818–156827. (Conference Name: IEEE Access)
- Feng, Z., Chen, S., Chen, Y., & Zheng, N. (2018, June). Model-Based Decision Making With Imagination for Autonomous Parking. In *2018 IEEE Intelligent Vehicles Symposium (IV)* (pp. 2216–2223). (ISSN: 1931-0587)
- Ferguson, D., Kalra, N., & Stentz, A. (2006, May). Replanning with RRTs. In *Proc. IEEE Int. Conf. Robotics and Automation ICRA 2006* (pp. 1243–1248).
- Ferguson, D., & Stentz, A. (2006, October). Anytime RRTs. In *Proc. IEEE/RSJ Int. Conf. Intelligent Robots and Systems* (pp. 5369–5375).
- González, D., Pérez, J., Milanés, V., & Nashashibi, F. (2016, April). A Review of Motion Planning Techniques for Automated Vehicles. *IEEE Transactions on Intelligent Transportation Systems*, *17*(4), 1135–1145.
- Jang, C., Kim, C., Lee, S., Kim, S., Lee, S., & Sunwoo, M. (2020, February). Re-Plannable Automated Parking System With a Standalone Around View Monitor for Narrow Parking Lots. *IEEE Transactions on Intelligent Transportation Systems*, *21*(2), 777–790.
- Jhang, J.-H., Lian, F.-L., & Hao, Y.-H. (2020, August). Forward and Backward Motion Planning for Autonomous Parking Using Smooth-feedback Bidirectional Rapidly-exploring Random Trees with Pattern Cost Penalty. In *2020 IEEE 16th International Conference on Automation Science and Engineering (CASE)* (pp. 260–265). (ISSN: 2161-8089)
- Jing, W., Feng, D., Zhang, P., Zhang, S., Lin, S., & Tang, B. (2018, November). A Multi-Objective Optimization-based Path Planning Method for Parallel Parking of Autonomous Vehicle via Nonlinear Programming. In *2018 15th International Conference on Control, Automation, Robotics and Vision (ICARCV)* (pp. 1665–1670).
- Karaman, S., & Frazzoli, E. (2011). Sampling-based algorithms for optimal motion planning. *The international journal of robotics research*, *30*(7), 846–894.
- Kuffner, J., & LaValle, S. (2000, April). RRT-connect: An efficient approach to single-query path planning. In *Proceedings 2000 ICRA. Millennium Conference. IEEE International Conference on Robotics and Automation. Symposia Proceedings (Cat. No.00CH37065)* (Vol. 2, pp. 995–1001 vol.2). (ISSN: 1050-4729)
- Kuwata, Y., Fiore, G. A., Teo, J., Frazzoli, E., & How, J. P. (2008, September). Motion planning for urban driving using RRT. In *Proc. IEEE/RSJ Int. Conf. Intelligent Robots and Systems* (pp. 1681–1686).
- Lavalle, S. M. (1998). *Rapidly-Exploring Random Trees: A New Tool for Path Planning* (Tech. Rep.).
- Li, B., Wang, K., & Shao, Z. (2016, November). Time-Optimal Maneuver Planning in Automatic Parallel Parking Using a Simultaneous Dynamic Optimization Approach. *IEEE Transactions on Intelligent Transportation Systems*, *17*(11), 3263–3274.
- Li, M. H., & Tseng, P. K. (2016, December). Implementation of an autonomous driving system for parallel and perpendicular parking. In *Proc. IEEE/SICE Int. Symp. System Integration (SII)* (pp. 198–203).
- Liu, W., Li, Z., Li, L., & Wang, F.-Y. (2017, December). Parking Like a Human: A Direct Trajectory Planning Solution. *IEEE Transactions on Intelligent Transportation Systems*, *18*(12), 3388–3397.
- Ortofoto Archiv. (n.d.). Retrieved 2020-01-21, from <http://app.iprpraha.cz/apl/app/ortofoto-archiv/>
- Petrov, P., & Georgieva, V. (2018, December). Geometric path planning and tracking control with bounded steering angle for the parking problem of automatic vehicles. *AIP Conference Proceedings*, *2048*(1), 060017. Retrieved 2019-11-05, from <https://aip.scitation.org/doi/abs/10.1063/1.5082132>
- RandyGaul, & Wizzard033. (2019). *cute_headers/cute_c2.h* [github]. Retrieved 2019-11-04, from https://github.com/RandyGaul/cute_headers/blob/master/cute_c2.h
- Reeds, J., & Shepp, L. (1990). Optimal paths for

- a car that goes both forwards and backwards. *Pacific journal of mathematics*, 145(2), 367–393.
- Robot Operating System*. (2023). Retrieved 2023-02-17, from <https://www.ros.org/>
- Sousa, B., Ribeiro, T., Coelho, J., Lopes, G., & Ribeiro, A. F. (2022, April). Parallel, Angular and Perpendicular Parking for Self-Driving Cars using Deep Reinforcement Learning. In *2022 IEEE International Conference on Autonomous Robot Systems and Competitions (ICARSC)* (pp. 40–46).
- Sucan, I. A., Moll, M., & Kavraki, L. E. (2012, December). The Open Motion Planning Library. *IEEE Robotics Automation Magazine*, 19(4), 72–82.
- Vlasak, J., Sojka, M., & Hanzálek, Z. (2019, October). Accelerated RRT* and Its Evaluation on Autonomous Parking. In (pp. 86–94). Retrieved 2019-10-31, from <http://www.scitepress.org/DigitalLibrary/Link.aspx?doi=10.5220/0007679500860094>
- Vlasak, J., Sojka, M., & Hanzálek, Z. (2022). Parallel Parking: Optimal Entry and Minimum Slot Dimensions. In *Proceedings of the 8th International Conference on Vehicle Technology and Intelligent Transport Systems* (pp. 300–307). Retrieved 2023-03-30, from <http://arxiv.org/abs/2205.02523> (arXiv:2205.02523 [cs])
- Vorobieva, H., Glaser, S., Minoiu-Enache, N., & Mammar, S. (2015, February). Automatic Parallel Parking in Tiny Spots: Path Planning and Control. *IEEE*, 16(1), 396–410.
- Wang, Y., Jha, D. K., & Akemi, Y. (2017, August). A two-stage RRT path planner for automated parking. In *2017 13th IEEE Conference on Automation Science and Engineering (CASE)* (pp. 496–502). (ISSN: 2161-8089)
- Zips, P., Böck, M., & Kugi, A. (2016, May). Optimisation based path planning for car parking in narrow environments. *Robotics and Autonomous Systems*, 79, 1–11. Retrieved 2020-02-21, from <http://www.sciencedirect.com/science/article/pii/S0921889016000294>
- Záhora, J., Hanzálek, Z., & Sojka, M. (2021, September). Perception, Planning and Control System for Automated slalom with Porsche Panamera. In *FISITA World Congress 2021 – Technical Programme*. FISITA. Retrieved 2023-04-12, from <https://www.fisita.com/library/fisita-world-congress/2021/f2020-acm-064>